The Meshless Radial Point Interpolation Method for Time-Domain Electromagnetics

Thomas Kaufmann, Christophe Fumeaux and Rüdiger Vahldieck
Laboratory for Electromagnetic Fields and Microwave Electronics - IFH
ETH Zurich, Zurich, CH-8092, Switzerland
Email: thomas.kaufmann@ifh.ee.ethz.ch

***Abstract*— A meshless numerical technique based on radial point interpolation is introduced for electromagnetic simulations in time domain. The general class of meshless methods presents very attractive properties for addressing future challenges of electromagnetic modeling. Among the interesting aspects, the ability to handle arbitrary node distributions for conformal and multi-scale modeling can be mentioned first. Furthermore, the possibility of modifying the node distribution dynamically opens new perspectives for adaptive computations and optimization. The mathematical background of the radial point interpolation method and a two-dimensional implementation are presented here. The advantages of this meshless method are discussed and applied to a model consisting of a 90 degree H-plane waveguide bend. It is shown that solutions converge much faster using the ability of conformal modeling compared to a similar analysis in rectangular grids.**

***Index Terms*— Meshless Methods, Time domain analysis, Radial Point Interpolation Method**

I. Introduction

This paper describes the implementation of a meshless simulation technique, the local radial point interpolation method (RPIM), as a time-domain solver for electromagnetics. Meshless methods provides unique advantages over conventional methods in numerical simulation of electromagnetic fields. Meshless methods do not require a detailed description of a mesh to perform numerical simulations, but are rather applied on a nearly arbitrary node distribution that describes the geometry of interest. A big advantage is the freedom in node placement which allows conformal modeling and provides multi-scale capabilities. A further advantage is the ability to move or add nodes, which facilitates dynamic adaptation of a model for increasing simulation accuracy, or changes in geometry for the optimization of structures. Finally, the potential of the method for multi-physics modeling is facilitated by the properties of the interpolation method, e.g. to include thermal, relativistic or quantum effects, or to describe semiconductors or plasmon gases.

Meshless methods are known in the fields of astrophysics and hydrodynamics for decades ([1], [2]). Many variations have emerged since then, e.g. Mean Least Squares (MLS) method, Smoothed Particle Hydrodynamics (SPH), or the reproducing kernel particle method (RKPM). In computational mechanics, RPIM was introduced in [3] and applied to electro- or magnetostatics, e.g. [4], [5]. An implementation for the collocation method in conjunction with wavelets was presented in [6]. Concerning electromagnetics, a meshless time-domain implementation based on SPH was recently presented in [7]. The interpolation method used in the present paper, i.e. RPIM, provides several advantages over SPH. First, RPIM is based on a local *support domain* instead of a global domain, which allows simulating large-scale problems. Second, the consistency of unevenly distributed nodal distributions is retained intrinsically in RPIM, which saves costly consistency restoring techniques. Third, no additional geometrical information such as the surrounding volume of a particular node is necessary.

In this paper we investigates some of the advantageous properties of RPIM in a specific example, a 90 degree H-plane waveguide bend. In this example conformal modeling provides great advantages in simulation accuracy and fast convergence, since stair-casing effects of the regular rectangular grids are avoided.

The paper is structured as follows. Sec. II gives a theoretical introduction to the local radial point interpolation method and its implementation to electromagnetics. The model under investigation and simulation results are described in Sec. III.

II. The RPI Method

The principle of the presently implemented meshless method relies on fundamental properties of the underlying interpolation method, i.e. the local radial point interpolation (RPI) method. The interpolation itself provides several advantages over other existing interpolation techniques, namely the ability to interpolate arbitrarily scattered data and its local nature [8]. This allows interpolating over unstructured node distributions and facilitates node adaptation at the cost of only a small overhead.

RPI provides a fitting curve for the instantaneous spatial distribution of the field components. A very interesting property of the interpolation is that the spatial derivatives can also be estimated accurately based on the same algorithm. Hence, partial differential equations can be solved in combination with a suitable scheme for time-derivatives. In

978-1-4244-1780-3/08/$25.00 © 2008 IEEE

the present case the discretized Maxwell curl equations are solved, but it should be mentioned that also other physical laws can be incorporated and solved in combination with Maxwell equations.

The field distribution around a particular node is interpolated locally by considering only a limited number of points within a local area, called support domain (Fig. 1). At the present stage of development the node distribution is assumed to remain unchanged during simulation, even though dynamic node adaptation techniques are considered for future work. Therefore, all interpolation parameters can be computed during preprocessing only, using the basis functions described in the following.

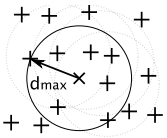

Fig. 1. Support domains of several nodes in the computational domain.

A. Interpolation Method

The radial basis point interpolation technique uses a combination of radial and monomial basis functions for the interpolation of the field distribution around a node. The approximation of a field component u is defined as follows:

$$\langle u(\mathbf{x})\rangle = \sum_{n=1}^{N} r_n(\mathbf{x})a_n + \sum_{m=1}^{M} p_m(\mathbf{x})b_m \qquad (1)$$

with $r_n(\mathbf{x})$ the radial basis function, $p_m(\mathbf{x})$ the monomial basis function, and a_n, b_n the associated interpolation coefficients. N is the number of points in the support domain and represents a relevant parameter of the RPI algorithm, which delimits the nearest neighbor search. M stands for the order of the monomial basis. In the present case linear monomial basis functions of the form $[\ 1 \quad x \quad y\ ]$ were chosen ($M = 3$). $\mathbf{x} = (x, y)$ is the position where the value of u is to be approximated. The angle brackets $\langle . \rangle$ denote the fact that this value is only an approximation of the actual field.

Several choices are possible as radial basis r_n, e.g. multiquadratics or spline functions. In the present implementation a Gaussian basis of the form $r(\mathbf{x}) = exp(-c|\mathbf{x}/d_{max}|^2)$ has been chosen for simplicity: A single parameter c controls the shape of the Gaussian basis. In the case of very large values for c, $r(\mathbf{x})$ converges towards the Dirac delta function. Equation (1) can be written in vector form as

$$\langle u(\mathbf{x})\rangle = \mathbf{r}^T(\mathbf{x})\mathbf{a} + \mathbf{p}^T(\mathbf{x})\mathbf{b} \qquad (2)$$

with the basis functions

$$\mathbf{r}^T(\mathbf{x}) = [\ r(\mathbf{x}_1), r(\mathbf{x}_2), \ldots, r(\mathbf{x}_N)\ ] \qquad (3)$$

$$\mathbf{p}^T(\mathbf{x}) = [\ 1 \quad x \quad y\ ]. \qquad (4)$$

The interpolation around the considered node is applied to all points in the support domain and can be written in matrix form

$$\langle \hat{\mathbf{u}} \rangle = \mathbf{R}_0\mathbf{a} + \mathbf{P}_0\mathbf{b} \qquad (5)$$

with $\hat{\mathbf{u}} = [u_1, ..., u_N]$ the interpolated values at the nodes in the support domain. The matrices $\mathbf{R}_0$ and $\mathbf{P}_0$ represent the basis functions evaluated at the positions of the N nodes

$$\mathbf{R}_0 = \begin{bmatrix} r_1(x_1, y_1) & \ldots & r_N(x_1, y_1) \\ \vdots & \vdots & \vdots \\ r_1(x_N, y_N) & \ldots & r_N(x_N, y_N) \end{bmatrix}_{N\times N} \qquad (6)$$

$$\mathbf{P}_0 = \begin{bmatrix} \mathbf{p}^T(x_1, y_1) \\ \vdots \\ \mathbf{p}^T(x_N, y_N) \end{bmatrix}_{N\times M}. \qquad (7)$$

The symmetry of $\mathbf{R}_0$ is given by the symmetric nature of the radial basis function. There are several ways to compute the coefficients $\mathbf{a}$, $\mathbf{b}$ from (5). The approach given by Wang et al. in [3] is applied here. To grant uniqueness of the solutions, constraints given in [9] are applied in the form of $\mathbf{P}_0^T\mathbf{a} = 0$. Combining the locally evaluated matrices $\mathbf{R}_0$ and $\mathbf{P}_0$ in a matrix $\mathbf{G}$, interpolation coefficients can be found according to

$$\underbrace{\begin{bmatrix} \mathbf{R}_0 & \mathbf{P}_0 \\ \mathbf{P}_0^T & \mathbf{0} \end{bmatrix}}_{\mathbf{G}} \begin{Bmatrix} \mathbf{a} \\ \mathbf{b} \end{Bmatrix} = \begin{Bmatrix} \mathbf{u^e} \\ \mathbf{0} \end{Bmatrix} \qquad (8)$$

$$\rightarrow \begin{Bmatrix} \mathbf{a} \\ \mathbf{b} \end{Bmatrix} = \mathbf{G}^{-1} \begin{Bmatrix} \mathbf{u^e} \\ \mathbf{0} \end{Bmatrix}. \qquad (9)$$

The vector $\mathbf{u^e} = [u_1, u_2, ..., u_N]^T$ holds the considered field component values of all nodes in the support domain. Taking a closer look at (8) and (9) reveals that the interpolation coefficients $\mathbf{a}$, $\mathbf{b}$ are obtained by multiplying the inverse of $\mathbf{G}$ with the values $\mathbf{u^e}$. Thus, introducing (9) in (5) with the matrix $\mathbf{G}^{-1}$, a shape function $\mathbf{\Psi}(\mathbf{x}) = [\Psi_1(\mathbf{x}), \Psi_2(\mathbf{x}), \ldots, \Psi_N(\mathbf{x})]$ can be defined in the following way:

$$\langle u(\mathbf{x})\rangle = [\ \mathbf{r}^T(\mathbf{x}) \quad \mathbf{b}^T(\mathbf{x})\ ]\mathbf{G}^{-1} \begin{Bmatrix} \mathbf{u^e} \\ \mathbf{0} \end{Bmatrix} = \mathbf{\Psi}(\mathbf{x})\mathbf{u^e}. \qquad (10)$$

The interpretation of (10) is that the interpolation of the field value at a specific node can be obtained by weighting the field values of the surrounding points with the shape function $\mathbf{\Psi}$. The shape function is only dependent on the values of the basis functions since $\mathbf{G}$ is considered constant within the support domain. The shape functions

describe a partition of unity within the local support domain and hence have to fulfill the following condition:

$$\sum_{n=1}^{N} \Psi_n(\mathbf{x}) = 1. \tag{11}$$

A powerful feature of the RPI algorithm is that it fulfills the following property for the spatial derivation

$$\langle \partial_\kappa u(\mathbf{x}) \rangle = [\ \partial_\kappa \mathbf{r}^T(\mathbf{x}) \quad \partial_\kappa \mathbf{b}^T(\mathbf{x})\ ] \mathbf{G}^{-1} \left\{ \begin{array}{c} \mathbf{u^e} \\ \mathbf{0} \end{array} \right\} = \partial_\kappa \mathbf{\Psi}(\mathbf{x}) \mathbf{u^e} \tag{12}$$

with $\kappa = x, y$. Therefore, since $\mathbf{G}$ remains unchanged, only the spatial derivatives of the basis functions are necessary to approximate $\partial_\kappa \mathbf{\Psi}(\mathbf{x})$. Consequently, also the spatial derivative of an interpolated field component can be retrieved as a linear combination of the field values of the nodes in the support domain.

The condition of the matrix $\mathbf{G}$ containing the locally evaluated basis functions is influenced by the number N of nodes in the support domain, the parameter c of the Gaussian basis function and the order M of the monomial basis. For example, increasing the parameter c to large values lets the Gaussian basis function converge towards the Dirac delta $\delta(\mathbf{x})$, and therefore the matrix $\mathbf{R}_0$ towards the identity matrix. This means that all nodes other than the node to be interpolated have no influence on the approximation, which decreases the accuracy of the algorithm. On the other hand values for c too small yield a nearly singular matrix $\mathbf{G}$ that cannot be inverted. It should be also mentioned that the choice of numbers of points in the support domain determines the size of $\mathbf{G}$ and thus heavily influences the computational effort necessary for the matrix inversion. A consequence of an improper choice for the above parameters is an ill-conditioned matrix $\mathbf{G}$. Numerical inversion of such a matrix is inaccurate and results in not fulfilling condition (11). Consequently, the simulation might become unstable independent of the chosen time-step. The characterization and determination of reliable parameters will be the focus of future communications.

B. Application to Electromagnetics

In the current paper a two-dimensional TE-mode implementation for the simulation of 2D waveguides is chosen for simplicity. As depicted in Fig. 2, the E-field is perpendicular and the H-fields are parallel to the propagation plane $\{x, y\}$. The nodes are staggered in space and time, which for a regular node distribution is similar to the 2D Yee cell. For a more general node distribution the spatial staggering is achieved starting from a specific node distribution for the E-nodes and applying a Voronoi decomposition to find H-nodes on the edges of the Voronoi cells. Both E and H node types can in principle be dynamically adapted during simulation.

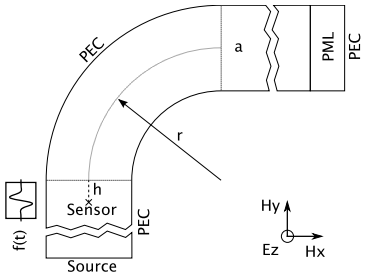

Fig. 2. Physical model of the 90 degree H-plane waveguide bend. The waveguide is specified as WR-229 and operates monomode from 3.22 GHz to 4.90 GHz. Dimensions are $a = 5.82$ cm and $r = 7.62$ cm.

Starting from the two-dimensional Maxwell curl formulation in time-domain, applying the approximations for the spatial derivations ($\partial_{x,y} \mathbf{\Psi}(\mathbf{x})$) and the leap-frog scheme for time-update yields

$$H_{x,i}^{n+\frac{1}{2}} = H_{x,i}^{n-\frac{1}{2}} - \frac{\Delta t}{\mu} \sum_j E_{z,j}^n \partial_y \Psi_j \tag{13}$$

$$H_{y,i}^{n+\frac{1}{2}} = H_{y,i}^{n-\frac{1}{2}} + \frac{\Delta t}{\mu} \sum_j E_{z,j}^n \partial_x \Psi_j \tag{14}$$

$$E_{z,i}^{n+1} = E_{z,i}^n + \frac{\Delta t}{\varepsilon} \left[\sum_j H_{y,j}^{n+\frac{1}{2}} \partial_x \Psi_j - \sum_j H_{x,j}^{n+\frac{1}{2}} \partial_y \Psi_j \right] \tag{15}$$

with i the updated node and j denoting the summation over N nodes in the support domain.

It is interesting to note that for a rectangular node distribution with constant distance and a support domain that contains four nodes, the shape functions take values that bring the scheme to the formulation of the finite-difference time-domain (FDTD) method.

Using a stability criterion similar to the CFL limit for FDTD yields stable simulations. The stability criterion is determined using the shortest distance $d_{min,i}$ between any two nodes in the computational domain:

$$\Delta t \leq \min_i (d_{min,i} \sqrt{\mu \varepsilon}). \tag{16}$$

III. Numerical Experiment

Numerical experiments have been performed in a 90 degree H-plane waveguide bend. This specific geometry has been chosen to illustrate one particular advantage of the meshless method, namely the ability to conformally model a geometry. The physical properties of the chosen waveguide are depicted in Fig 2.

In order to evaluate the performance of the RPI method, a conformal node distribution is applied using a constant node spacing in r- and φ- direction of the bend (Fig. 3(a)). Before and after the bend, a regular rectangular node

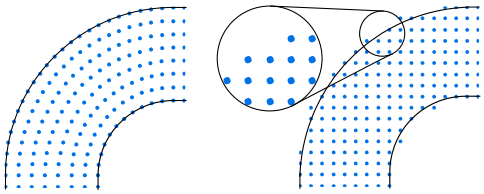

(a) Conformal model approximation with meshless method

(b) Rectangular regular grid similar to Yee-scheme in FDTD

Fig. 3. Comparison of discretizations using conformal or regular node distribution.

distribution is applied. Using such a node placement allows correct modeling of the curved perfect electric conductor (PEC) at the waveguide boundaries. This conformal nodal distribution is compared to a fully regular rectangular node distribution with different discretizations (Fig. 3(b)). The support domain for the presented numerical experiments has been set to include a minimum of $N \geq 4$ nodes.

Both node distributions are expected to converge with increased node density. For the conformal model reliable results should be achieved for relatively coarse discretizations already. For regular node distributions stair-casing effects will pose problems for coarse discretizations. Thus comparable results can be expected for very fine discretization where the physical model is properly approximated. The parameter investigated, the voltage standing wave ratio (VSWR), is numerically measured by recording the field values at the sensor location shown in Fig. 2 with a distance of $h = 7.14$ cm from the bend. To compute the VSWR of the bend, the recorded fields are compared to a reference solution provided by a very long straight waveguide in positive y-direction. Simulations were performed for discretizations $[\lambda/8, \lambda/17, \lambda/26, \lambda/34, \lambda/43]$ where λ corresponds to the freespace wavelength of the highest operation frequency (4.9 GHz). Fig. 4(a) shows the convergence for the regular node distribution. Due to stair-casing effects, a very fine discretization of at least $\lambda/43$ is required to achieve reliable simulation results. The results in Fig. 4(b) on the other hand converge much faster. For discretizations finer than $\lambda/17$ no significant improvement can be seen.

IV. Conclusion

A meshless method for numerical electromagnetic analysis, the RPI method, has been introduced and discussed. An overview of the mathematical properties has been given. As illustration a two-dimensional implementation for TE-modes has been used to simulate the input reflections of a 90 degree H-plane waveguide bend. It could be confirmed that the ability for arbitrary node placement significantly increases the simulation accuracy over the usage of conventional rectangular grids. The VSWR converges much faster in the case of conformal node placement

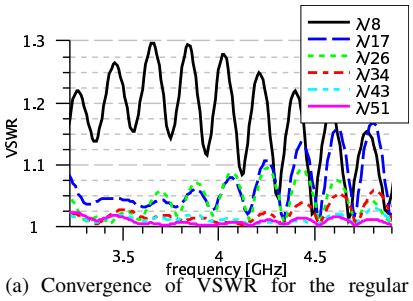

(a) Convergence of VSWR for the regular rectangular node distribution.

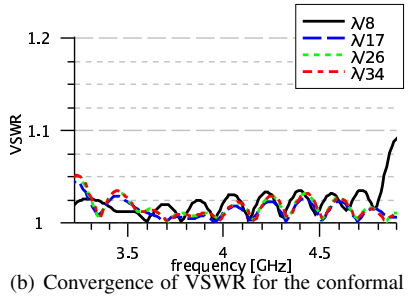

(b) Convergence of VSWR for the conformal node distribution.

Fig. 4. Convergence for the VSWR in rectangular and conformal grid.

compared to the results in the rectangular grid where stair-casing effects impair the simulation accuracy.

In a future investigations, steps towards the development of adaptive grid adaptation techniques will be taken to achieve a numerical method with dynamic increase of accuracy.

References

[1] J. J. Monaghan, "Smoothed particle hydrodynamics," *Annual review of astronomy and astrophysics*, vol. 30, pp. 543–574, 1992.

[2] T. Belytschko, Y. Krongauz, D. Organ, M. Fleming, and P. Krysl, "Meshless methods: An overview and recent developments," *Computer Methods in Applied Mechanics and Engineering*, vol. 139, no. 1-4, pp. 3–47, 1996.

[3] J. G. Wang and G. R. Liu, "A point interpolation meshless method based on radial basis functions," *International Journal for Numerical Methods in Engineering*, vol. 54, no. 11, pp. 1623–1648, 2002.

[4] S. Ho, S. Yang, J. Machado, and H. Wong, "Application of a meshless method in electromagnetics," *Magnetics, IEEE Transactions on*, vol. 37, no. 5, pp. 3198–3202, Sep 2001.

[5] G. R. Liu, K. Y. Dai, K. M. Lim, and Y. T. Gu, "A radial point interpolation method for simulation of two-dimensional piezoelectric structures," *Smart Materials and Structures*, vol. 12, no. 2, pp. 171–180, 2003.

[6] S. Ho, S. Yang, H. Wong, and G. Ni, "A meshless collocation method based on radial basis functions and wavelets," *Magnetics, IEEE Transactions on*, vol. 40, no. 2, pp. 1021–1024, March 2004.

[7] G. Ala, E. Francomano, A. Tortorici, E. Toscano, and F. Viola, "Smoothed particle electromagnetics: A mesh-free solver for transients," *Journal of Computational and Applied Mathematics*, vol. 191, no. 2, pp. 194–205, 2006.

[8] M. D. Buhmann, *Radial Basis Functions*. Cambridge University Press, 2003.

[9] M. Golberg, C. Chen, and H. Bowman, "Some recent results and proposals for the use of radial basis functions in the BEM," *Engineering Analysis with Boundary Elements*, vol. 23, no. 4, pp. 285–296, 1999.